Developmental Biology 407 (2015) 145–157

Contents lists available at ScienceDirect

Developmental Biology

journal homepage: www.elsevier.com/locate/developmentalbiology

Cadherin-11 coordinates cellular migration and extracellular matrix remodeling during aortic valve maturation

Caitlin J. Bowen [1], Jingjing Zhou [1], Derek C. Sung, Jonathan T. Butcher *

Department of Biomedical Engineering, Cornell University, United States

ARTICLE INFO

Article history:
Received 14 February 2015
Received in revised form
15 June 2015
Accepted 13 July 2015
Available online 16 July 2015

Keywords:
RhoA
Stress fiber
Compaction
Filopodia
Hyperplasia
Aortic valve insufficiency
Congenital heart defect
Calcification

ABSTRACT

Proper remodeling of the endocardial cushions into thin fibrous valves is essential for gestational progression and long-term function. This process involves dynamic interactions between resident cells and their local environment, much of which is not understood. In this study, we show that deficiency of the cell–cell adhesion protein cadherin-11 (Cad-11) results in significant embryonic and perinatal lethality primarily due to valve related cardiac dysfunction. While endocardial to mesenchymal transformation is not abrogated, mesenchymal cells do not homogeneously cellularize the cushions. These cushions remain thickened with disorganized ECM, resulting in pronounced aortic valve insufficiency. Mice that survive to adulthood maintain thickened and stenotic semilunar valves, but interestingly do not develop calcification. Cad-11 $^{-/-}$ aortic valve leaflets contained reduced Sox9 activity, β1 integrin expression, and RhoA-GTP activity, suggesting that remodeling defects are due to improper migration and/or cellular contraction. Cad-11 deletion or siRNA knockdown reduced migration, eliminated collective migration, and impaired 3D matrix compaction by aortic valve interstitial cells (VIC). Cad-11 depleted cells in culture contained few filopodia, stress fibers, or contact inhibited locomotion. Transfection of Cad-11 depleted cells with constitutively active RhoA restored cell phenotypes. Together, these results identify cadherin-11 mediated adhesive signaling for proper remodeling of the embryonic semilunar valves.

1. Introduction

Heart valves are critical regulators of one-way blood flow through the heart. The embryonic heart grows nearly 100 fold during embryonic development, developing similar increases in ventricular chamber pressures that require continuous valve action for gestational progression (Butcher et al., 2007b; Hu and Clark, 1989; Keller et al., 1991). The valvular primordia originate from the endocardium of the atrioventricular (AV) and outflow tract (OFT) through a process of endocardial to mesenchymal transformation (EMT). The new mesenchymal cells invade and proliferate into an underlying gelatinous matrix called the cardiac jelly, until a nearly homogenous cellularized mass is formed (Moreno-Rodriguez et al., 1997). Well over 100 molecular agents coordinate to govern EMT decisions and subsequent cushion formation (Chakraborty et al., 2010; Eisenberg and Markwald, 1995; Person et al., 2005; Townsend et al., 2011). Defects in the early EMT process in valves are nearly uniformly lethal and unlikely to be registered clinically (Bartman and Hove, 2005). However, defects in the subsequent remodeling of the valvuloseptal apparatus are the most common type of birth defect (affecting 1–2% of all live births) and often requires intervention soon after birth (Hoffman et al., 2004). Therefore, an understanding of these later stage mechanisms is critically important for generating clinically relevant intervention strategies.

After cardiac chamber septation, the globular AV and OFT cushions condense and elongate into thin fibrous leaflets. The glycosaminoglycan rich extracellular matrix of the cushion is remodeled into highly organized stratified layers: the ventricularis (or atrialis in the case of the AV valves) containing a laminate of collagen and elastin, the spongiosa layer retaining mostly proteoglycans, and the fibrosa containing a mesh network of dense collagen bundles (Aikawa et al., 2006; Hinton et al., 2006; Kruithof et al., 2007). These layers work together for efficient biomechanical function of the leaflets, and consequently function is impaired when this matrix organization is compromised (Sacks and Schoen, 2002). Simultaneous with this matrix remodeling, the highly proliferative, immature, mesenchymal progenitors of the cushion mature into a low-proliferative fibroblast-like phenotype. Far less is known about the mechanisms that control these later remodeling events. Much attention has been given to identifying upstream growth factors and downstream transcription factors that are involved. A common phenotypic outcome resulting from a

* Corresponding author. Fax: +1 607 255 7330.
E-mail address: jtb47@cornell.edu (J.T. Butcher).
[1] These authors contributed equally to this work.

http://dx.doi.org/10.1016/j.ydbio.2015.07.012
0012-1606/

variety of disparate genetic mutations in mouse models is a hyperplastic cushion with failure to condense or form quiescent fibroblasts. This can result from mutations in TGFβ, VEGF, BMP, or other pathways (Azhar et al., 2011; Galvin et al., 2000; Lee et al., 2006), which suggests that all of these factors integrate, albeit complexly, into cellular decisions to interact with and remodel their microenvironment.

Cell-matrix adhesive interactions are governed largely by complexes involving integrin receptors, while cell–cell adhesion is governed primarily by cadherin containing complexes. We and others have previously shown that both migration and matrix condensation by AV cushion mesenchyme is adhesion dependent (Butcher et al., 2007a; Ghatak et al., 2014; Mo and Lau, 2006). The disruption of adherens junctions formed by endothelial/epithelial cadherins, VE-cadherin, and E-cadherin are critical for the initiation of EMT (Tatin et al., 2013). Cadherins are also present in mesenchymal cells, and perform key roles coordinating collective migration behaviors during embryonic development (Theveneau et al., 2010).

Cadherin-11 (also Cad-11, cdh-11, OB-cadherin) is a mesenchymal cadherin that is expressed at the interface of tissues that acquire fibroblastic and osteoblastic phenotypes (Hoffmann and Balling, 1995; Simonneau et al., 1995). Dysregulated Cad-11 expression contributes to inflammation, cartilage degradation, and metastasis in diseases such as pulmonary fibrosis, rheumatoid arthritis, and multiple cancer types (Assefnia et al., 2014; Lee et al., 2007; Schneider et al., 2012; Tomita et al., 2000). Cad-11 also plays important roles in both cellular migration and differentiation in development, in particular through mediating collective migration and fate specification in neural crest mesenchyme (Becker et al., 2013; Borchers et al., 2001; Kashef et al., 2009). We recently profiled the spatial and temporal expression of cadherin-11 (Cad-11) during murine heart valve development (Zhou et al., 2013). Cad-11 is expressed throughout the early cushion mesenchyme, but its expression decreases and is redistributed in to the endothelial cell layer during the later remodeling period as valves condense and elongate into leaflets. These results motivated our hypothesis that Cad-11 regulates the cellular architecture of the endocardial cushion and participates in its subsequent remodeling and phenotype maturation.

Here, we studied the effects of Cad-11 depletion on embryonic valve formation and remodeling in vitro and in vivo. We establish that Cad-11 is dispensable for EMT, but essential for proper cellularization of the cushion. Cad-11 mutant semilunar valves remain thickened, do not form an organized extracellular matrix, and result in significant lethality secondary to insufficiency. Cad-11 deletion/knockdown disrupts valvular cell polarity, stress-fiber formation, migration, and matrix compaction. We further found that Cad-11 depletion reduces RhoA activity mediated filopodia protrusion. Treatment of Cad-11 deficient valve interstitial cells with constitutively active RhoA restored all these cellular behaviors. Together, these results demonstrate that Cad-11 is essential for establishing and coordinating embryonic valve mesenchymal cell activities though RhoA to create mature fibrous leaflets.

2. Materials and methods

2.1. Mouse strains

Wildtype C57BL/6 and Cad-11 $^{-/-}$ mice (Taconic Biosciences) were bred according to standard protocols. Cad-11 $^{-/-}$ mice were donated by Michael Brenner and Masatoshi Takeichi (Kawaguchi et al., 2001). All animal work was conducted following national and international research guidelines. Full details of this study were reviewed and approved by the Cornell IACUC (protocol #2008-0011).

2.2. Histology and immunofluorescence labeling

Embryos and adult hearts were fixed in 4% paraformaldehyde overnight at 4 °C, then dehydrated through an ethanol series and paraffin embedded and sectioned at 8 μm thickness. Following dewaxing and rehydration, sections were stained with Hematoxylin and Eosin (H&E, cellular composition), Von Kossa (phosphate), Alcian Blue (glycosaminoglycans), Picrosirius red (collagen), and Verhoeff-Van Geison (elastin). TUNEL reaction was carried out as described in Gould et al. (2012). For BrdU immunohistochemistry, E16.5 embryos were sacrificed 2 h after IP injection of 1 mg of BrdU reagent (BD Biosciences). Nuclear DNA was denatured in 2 N hydrochloric acid for 10 min at 37 °C and quenched with hydrogen peroxide for 10 min at room temperature. Sections were incubated in primary antibodies (1:100) overnight at 4 °C, and then in secondary antibodies (1:300) for 1 h at a room temperature. 3,30-Diaminobenzidine (DAB) was used as a chromogen. The percent of positive cells was determined by normalizing to the total cell number for both TUNEL and BrdU staining assays. Relative cushion area was calculated by taking the largest cushion area from serial sections, and normalizing to wild type cushion size at E11.5. Cell fraction vs. depth fraction was determined by counting the number of cells at serial distances away from the myocardial edge of the cushion, and normalizing to total cell number and cushion size at E18.5. Valve thickness was measured using the widest thickness of a valve leaflet from serial sections at E18.5. To measure stain intensity for histological stainings, first the ImageJ plugin Color Deconvolution was used for the appropriate stain, then intensity was measured and normalized to a tissue control portion of the section, such as bone for Alcian Blue or arterial wall for Verhoeff-Van Geison stains. Calcification density was determined by calculating the size of any lesions present relative to the valve leaflet size, and normalizing to lesion percentages in wild type valve leaflets. Additional sections were processed for immunohistochemistry. For immunodetection, 10 mM citrate buffer was used for antigen retrieval, and sections were blocked with 10% goat serum before primary antibodies (1:100 dilution) were used against Sox9 (rabbit, Abcam), vimentin (mouse, Invitrogen), alpha-smooth muscle actin (mouse, Sigma), Active RhoA-GTP (mouse, NewEast Biosciences), and β1 integrin (mouse, BioGenex). Fluorescence-conjugated Alexa Fluor 488 goat anti-rabbit and Alexa Fluor 568 goat anti-mouse secondary antibodies (Invitrogen, 1:200 dilution) were used according to the primary antibody species. Sections were nuclei counterstained with DRAQ5 (Abcam, 1:1000 dilution). Signals were detected and images were collected with Zeiss 710 confocal microscopy (Cornell University Life Sciences Core Laboratories Center). Nuclei (blue) were counted manually to determine cell number, and normalized to the size of the leaflet. The widest valve sections were used for these calculations to ensure consistency. Immunoreactivity of proteins stained in tissue sections was measured using ImageJ (NIH, Bethesda, MD) as demonstrated previously, with expression normalized to valve size and immunofluorescence intensity of wild type valve regions (Farrar and Butcher, 2013; Mahler et al., 2013). Sox9 nuclear co-localization was measured using NIH ImageJ software. Green (Sox9) and far-red (nuclei) channels were each thresholded and co-localized regions were measured using the ImageJ plugin Co-localization. Fluorescence intensity of colocalized Sox9 was taken as a percentage of overall Sox9 fluorescence intensity.

2.3. Doppler ultrasound transthoracic echocardiography

Mice were bred according to standard protocol, and plug checks were used to determine day of pregnancy. Embryos and mice were bred to desired stage, and the mice were anesthetized using 1.5% isoflurane. Abdomens of pregnant females and chests of

adult mice were treated with a chemical hair remover to reduce attenuation. Heart rate and core temperature were continuously monitored throughout the procedure. 2D cross-sectional and Doppler transthoracic echocardiography was performed using a Visual Sonics Vevo 2100 system (Cornell University Life Sciences Core Laboratories Center).

2.4. Genetic modification of cells

Porcine aortic valve interstitial cells (PAVICs) were cultured in Dulbecco's modified Eagle's medium (Invitrogen, Carlsbad, CA) supplemented with 5% fetal bovine serum (Gibco, Grand Island, NY) at 37 °C and 5% CO_2 as previously described (Butcher and Nerem, 2004). PAVICs were used between passages 5–8. PAVICs or primary culture chick interstitial valve cells were transfected with plasmids using the Neon Transfection system (Invitrogen) for one pulse at 1600 V for 20 ms. Cells were transfected with three scrambled control plasmids, three Cad-11 short interfering RNA (siRNA) plasmids, or three Cad-11 siRNA plasmids and a constitutively active RhoA (CA-RhoA) plasmid (pRK5-myc-RhoA-Q63L was a gift from Gary Bokoch, Addgene plasmid # 12964) (Table S1). RNA was extracted using the RNeasy Mini Kit (Qiagen, Valencia, CA) and reverse transcribed into cDNA using the SuperScript III Reverse Transcriptase kit (Invitrogen) according to the manufacturer's instructions. Gene expression and Cad-11 knockdown was confirmed using real-time PCR (qPCR) with custom primers (Table S2) and SYBR Green PCR master mix. Transfected cells were seeded on autoclaved glass slides and cultured for 48 h. They were subsequently fixed with 4% paraformaldehyde at room temperature, permeabilzed with 0.2% Triton-X, and blocked with 10% goat serum before staining with phalloidin conjugated with Alexa Fluor 488 (F-actin, Invitrogen, 1:40 dilution) and DRAQ5.

2.5. Valve cell explant migration, compaction, and morphology

HH24 AV cushion or HH40 aortic valve leaflet cells were isolated from chick hearts and cultured before use in migration and compaction assays as previously described (Butcher et al., 2007a). For migration, HH24 chick interstitial valve cells were collected in a hanging drop culture before seeding in a 1% collagen gel. Migration area was measured by outlining the region of maximum migration in all directions. HH40 chick interstitial valve cells were seeded within a 1% collagen gel at 400,000 cells/ml and gels were allowed to compact for 7 days. To examine migration and cell morphology, Cad-11 $^{-/-}$ and wildtype mouse aortic valve interstitial cells were isolated from hearts and explanted on 1% collagen hydrogels. Cells were allowed to migrate for 24 h before being fixed with 4% paraformaldehyde at room temperature, permeabilized with 0.2% Triton-X, and blocked with 10% goat serum before staining with phalloidin (F-actin) conjugated with Alexa Fluor 488 (1:40 dilution, Invitrogen). To study morphological differences, cells were allowed to adhere for 48 h before being fixed with 4% paraformaldehyde at room temperature, permeabilzed with 0.2% Triton-X, and blocked with 10% goat serum before staining with Active RhoA primary antibody and Alexa Fluor 488 secondary antibody or phalloidin conjugated with Alexa Fluor 488 (F-actin, Invitrogen, 1:40 dilution). Genetically modified PAVICs were cultured on glass slides immediately after siRNA treatment for 48 h and stained with phalloidin. Protrusion length and number were manually counted and measured from tip to base. Similarly, the number of cells with stress fibers were manually counted and taken as a percentage of total number of cells in a given image area. Overlapping cells were categorized as cells that were both touching and on top of other cells, normalized to total cell number in a given image area.

2.6. Statistical analyses

All data are reported as means with at least three independent experiments per treatment, and error bars represent standard error of the mean. Statistical significance was determined using the Student's *t*-test or Chi-squared analysis. Differences between means were considered significant at $p < 0.05$.

3. Results

3.1. Cad-11 deletion results in embryonic and perinatal lethality

Previously, our group showed that Cad-11 expression is spatially and temporally restricted to developing heart valves (Zhou et al., 2013). Though Cad-11 $^{-/-}$ mice are viable, they have small litters at birth and the Cad-11 $^{-/-}$ mice are smaller in size than their siblings. We therefore suspected the existence of a cardiovascular defect. We acquired and genotyped litters between E10.5 and the perinatal period (P2). Wildtype mice were present at expected Mendelian ratios throughout development. Homozygous Cad-11 null (Cad-11 $^{-/-}$) mice exhibited significant lethality both at E12.5 and at birth (Table 1, $p=0.02$, 1.00E−7, respectively). The most dramatic Cad-11 $^{-/-}$ lethality occurred between E14.5 (68% of expected survival) and birth (24% of expected survival, $p=1.00E-7$), suggesting that Cad-11 plays a functional role during these stages of development. We also found evidence of liver hemorrhaging in E12.5 mice, which is consistent with pronounced cardiac dysfunction (Sakata et al., 2002) (Fig. S1).

3.2. Cad-11 $^{-/-}$ embryos exhibit structural defects in valve morphogenesis in early and late gestation

Histological analysis revealed that the atrioventricular endocardial cushions at E11.5 were approximately 36% smaller than wildtype controls (Cad-11 $^{+/+}$), while the outflow tract cushions were similar in size (Fig. 1A and B). Interestingly, Cad-11 $^{-/-}$ AV cushions contained an uneven cellular distribution, with 74% more cells concentrated toward the endocardial surface of the atrioventricular and outflow tract cushions. These results suggest that Cad-11 deletion does not disrupt endocardial to mesenchymal transformation, but rather impairs the subsequent migration of these mesenchymal cells through the cushions (Fig. 1C, Fig. S1G). Interestingly, by stage E18.5, the semilunar valves of Cad-11 $^{-/-}$ hearts were significantly thickened (> 65%) compared with those of wildtype controls, while the atrioventricular valves were similar in size and shape (Fig. 1A and D). These results suggest that post-EMT remodeling of the valves derived from the outflow tract cushion may be more affected by the loss of Cad-11, as the valves that developed from the misaligned atrioventricular cushions were able to recover and develop properly. Additionally, there are post-EMT remodeling contributions from multiple cell types in the outflow tract that are absent from the atrioventricular tract, such as neural crest and anterior heart field mesenchyme (Lin et al., 2012), which may also be affected by loss of Cad-11. To assess the consequence of the dysmorphic aortic valve on cardiac function, Doppler in utero echocardiography was performed on the aortic valve of E17.5 embryos. Cad-11 $^{-/-}$ aortic valves exhibit significant regurgitant flow, averaging 47% of forward flow (Fig. 2A). Together, these results identify that Cad-11 is required for proper functional remodeling of the semilunar valves. Although pulmonary valve morphology was also affected, we did not further investigate it at this time as the aortic valve is of greater clinical significance given its role in mediating cardiac output and is far likelier to contribute to embryonic and post-natal lethality.

Table 1
Loss of Cad-11 significantly impairs embryonic survival. Cad-11 $^{+/-}$ mice were crossed to generate litters with mixed genotypes. The resulting number of each genotype is shown with the corresponding percentage given in parentheses. At all stages, the expected percentage is the Mendelian ratio of 25%/50%/25%. E designates embryonic day. *p*-Values calculated by chi-squared analysis at stage E12.5 and at birth are statistically significant, suggesting that it is just prior to these points the embryos are unable to survive.

	Cad11 $^{+/+}$	Cad11 $^{+/-}$	Cad11 $^{-/-}$	*p*-Value
E10.5	20 (29%)	31 (46%)	17 (25%)	0.67
E12.5	20 (40%)	17 (34%)	13 (26%)	**0.02**
E14.5	5 (17%)	19 (66%)	5 (17%)	0.24
Birth	56 (39%)	77 (54%)	9 (6%)	**1.00E−7**

3.3. Cad-11 deficiency affects the extracellular matrix remodeling of fetal aortic valve leaflets

The structural anomalies in aortic valves of Cad-11 $^{-/-}$ mice suggested defects in cellularization and/or matrix remodeling. We first assessed proliferation and apoptosis during late stage aortic valve remodeling (E16.5). Mutant valves exhibited no differences in cell proliferation as compared to control valves, and there were very few apoptotic cells in either control or mutant valve regions at this stage (Fig. S1). We next characterized the extracellular matrix composition of late stage aortic valve cusps in Cad-11 $^{-/-}$ embryos. Cad-11 $^{-/-}$ aortic valves express significantly lower levels of glycosaminoglycans (GAGs) than controls (Fig. 2B and C). No discernable changes in elastin or collagen content were observed in comparison to controls (Fig. S2). We then profiled the expression of Sox9, a transcription factor important for valvulogenesis and known to stimulate glycosaminoglycan synthesis (Lincoln et al., 2007). E18.5 Cad-11 $^{+/+}$ aortic valves express Sox9 prominently (cytoplasmic and nuclear) in the endocardium and the VIC in close proximity. In E18.5 Cad-11 $^{-/-}$ aortic valves, Sox9 expression was markedly decreased and rarely nuclear (27.6 $^{+/-}$ 3.5% vs. 11.8 $^{+/-}$ 3.2%, $p < 0.05$, Fig. 2D and E). These results suggest that Cad-11 affects the cellular patterning and subsequent extracellular matrix remodeling of the aortic valve.

3.4. Cad-11 knockdown decreases avian endocardial migration and compaction

To dissect the cellular mechanisms underlying the endocardial cushion and valve defects with Cad-11 deficiency, we applied siRNA knockdown of Cad-11 to primary isolated chick aortic valve (AoV) cells, consistently achieving $>65\%$ knockdown (Fig. 3A). To evaluate the role of Cad-11 on AoV mesenchymal cell migration, Cad-11 siRNA and scrambled siRNA control treated HH24 AoV

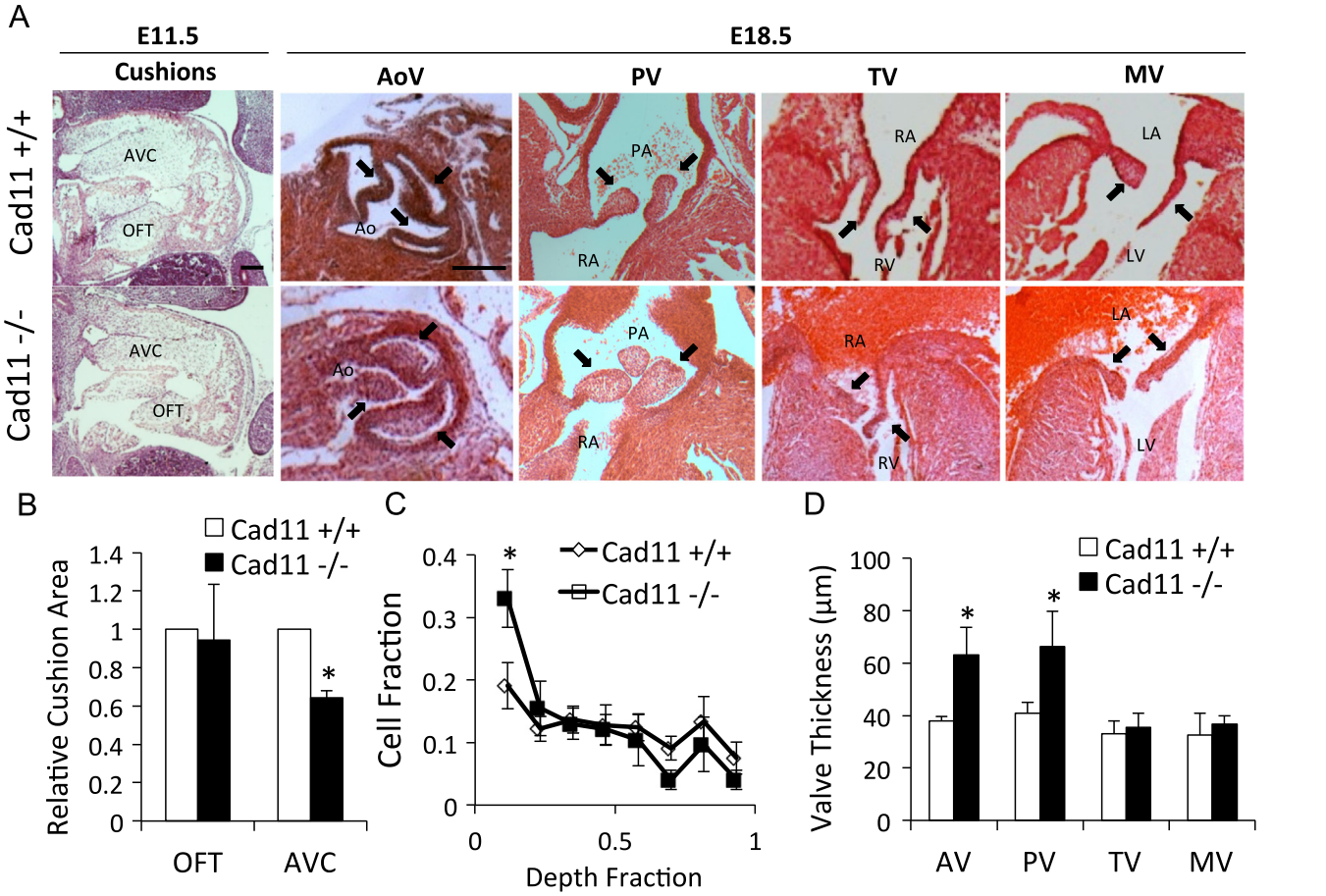

Fig. 1. Deletion of Cad-11 causes atrioventricular cushion defects at E11.5 and semilunar valve defects at E18.5 in mice. (A) Cad-11 null atrioventricular cushions are smaller than control at E11.5. Cad-11 null aortic and pulmonary valve leaflets are larger than control leaflets but tricuspid and mitral valve leaflets are similarly sized in both cad-11 null and control mice at E18.5. (Scale bar=0.1 mm) (B) Quantification of AV cushion sizes at E11.5 ($n=6$, $p<0.05$). (C) Cad-11 null valves have an uneven distribution of cells within the atrioventricular cushion at E11.5, with more cells closer to the endothelial edge of the cushion, ($n=7$, $p<0.05$ for KO depth, $p>0.05$ for WT cushions). (D) Quantification of heart valve leaflet thickness at E18. 5 ($n=6$, $p<0.05$). AVC=atrioventricular canal; OFT=outflow tract; Ao=aorta; PA=pulmonary artery; RA=right atrium; RV=right ventricle; LA=left atrium; LV=left ventricle; Arrows indicate valve leaflets.

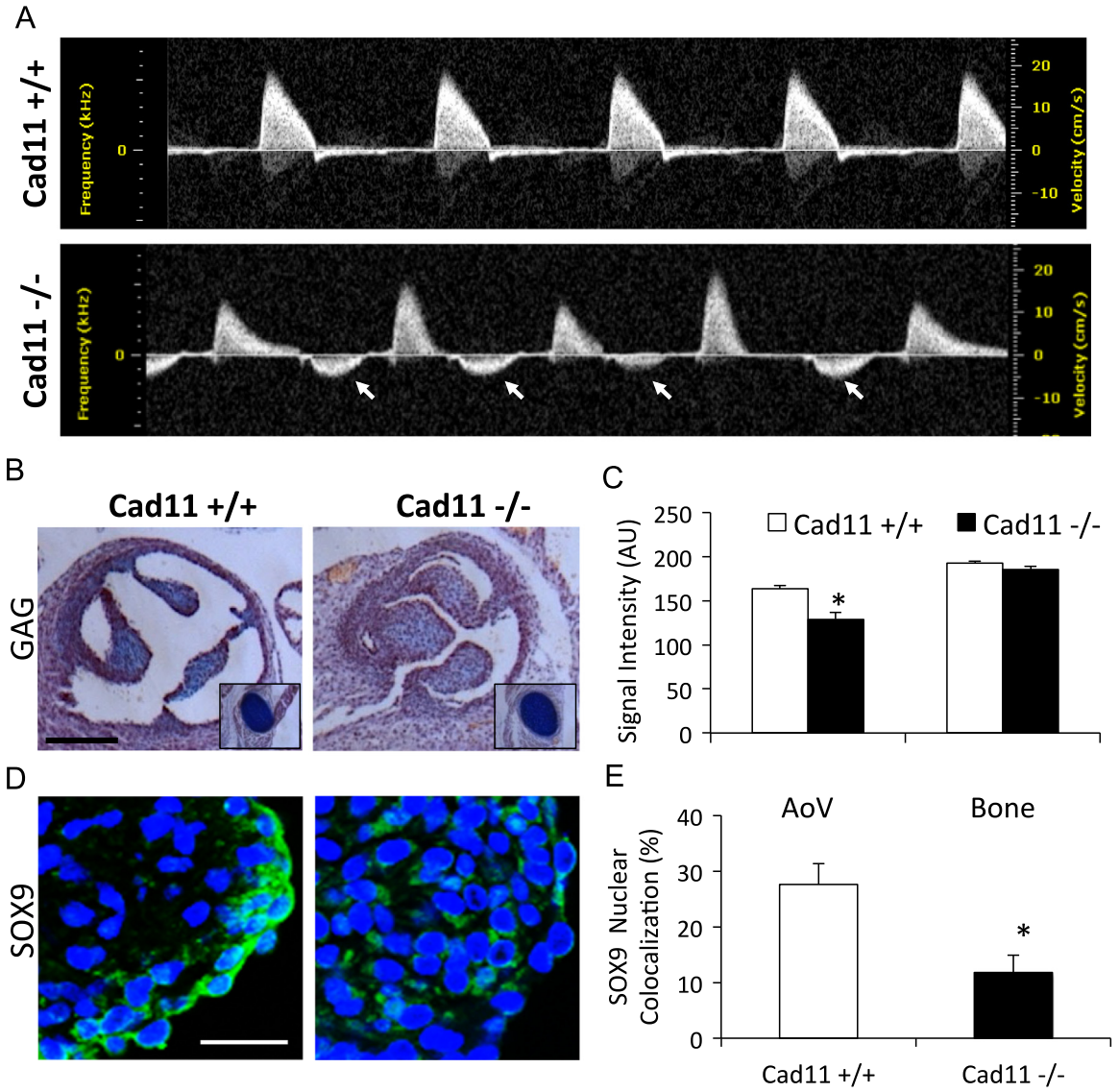

Fig. 2. Cad-11 null embryos have reduced GAGs and nuclear SOX9 in aortic valve leaflets at E18.5, and display embryonic valvular regurgitation. (A) Echocardiography using pulse-wave Doppler ultrasound shows that defective valve morphology causes regurgitation of blood flow through the aortic valve in late stages of embryonic development, suggesting a functional deficiency for lethality. Regurgitation is characterized by negative flow velocity (white arrows), which is not present in wild type embryos. (B, C) Alcian blue staining shows decreased GAGs in Cad-11 null mouse aortic valves as compared to control valves at E18.5. Boxed regions are positive Alcian blue staining in bones of Cad-11 null and control mice ($n=3$, $^{*}p<0.05$). Scale bar=100 μm (D, E) SOX9 is more highly colocalized with nuclei in wild type mice suggesting it is active as opposed to Cad-11 null mice, where it is expressed mostly in the cytoplasm ($n=6$, $^{*}p<0.01$) Scale bar=25 μm.

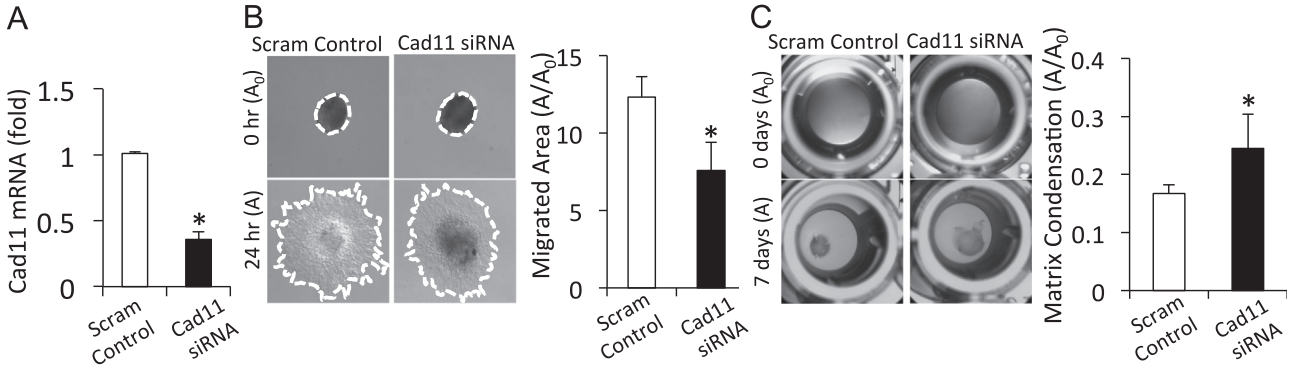

Fig. 3. (A) Quantification of Cad-11 mRNA expression in chick HH24 AV cushions confirms siRNA knockdown efficiency. Knockdown of Cad-11 impairs cell migration of embryonic cushion mesenchyme and impedes ECM compaction of fetal valve mesenchyme. (B) Chick HH24 AV cushions transfected with Cad-11 siRNA plasmids migrate less compared to scramble controls after 24 h and quantification of cushion cell migration size at HH24 ($n=4$, $p<0.01$). (C) Cad-11 knocked down aortic valve interstitial cells compact less than control cells after 7 days of culture at HH40 and quantification of aortic valve interstitial cell matrix condensation at HH40. ($n=4$, $p<0.05$).

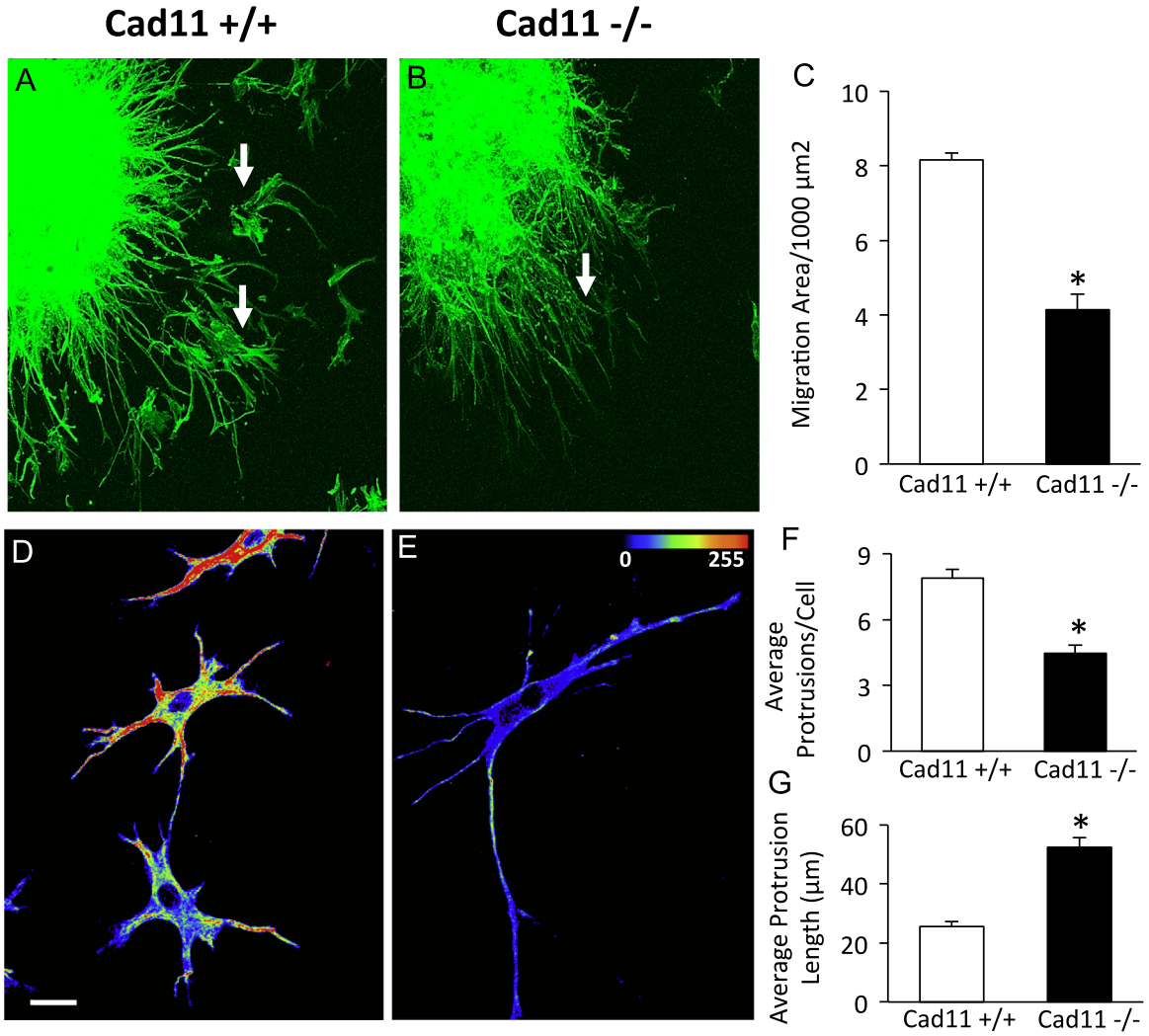

Fig. 4. Cad-11 null mouse valve cells have longer and fewer protrusions, express less active RhoA and migrate less in collagen hydrogels. (A, B) Cad-11 null cells (B) show reduced migration in collagen hydrogels compared to control cells (A). F-actin staining (green) shows Cad-11 null cells have different cell protrusion morphology at the migrating edges and that cells are unable to detach and migrate away from the initial condensed hanging drop culture, whereas control cells are able to migrate as whole cells (white arrows). (C) Quantification of Cad-11 null valve interstitial cell migration area. ($n=4$, $^*p<0.05$). (D, E) Cad-11 null cells (E) have less active RhoA compared to control cells (D) at the edges, shown as fluorescence intensity scaled 0 to 255. Scale bar=50 μm (F) Quantification of cell protrusion numbers of wildtype and Cad-11 null aortic valve interstitial cells ($n=20$, $^*p<0.05$). (G) Quantification of cell protrusion lengths of wildtype and Cad-11 null aortic valve interstitial cells ($n=20$, $^*p<0.05$).

mesenchymal cells were aggregated by hanging drop and placed on top of a collagen I gel. Cad-11 siRNA treated AoV mesenchyme migrated ~38% less than cells control cells ($p<0.05$, Fig. 3B). These results were also repeated with murine aortic valve interstitial cells from Cad-11 WT and Cad-11 $^{-/-}$ mice (Fig. 4). As in the embryonic condition, Cad-11 deficient VIC migrated roughly half the distance of the WT cells (Fig. 4A–C). Interestingly, while normal VIC exhibited collective migration away from the central cell mass, while Cad-11 knockdown cells were unable to separate away (Fig. 4A vs. B). Next, we assessed the affect of Cad-11 in a model of cellular traction force mediated extracellular matrix compaction (Grinnell et al., 1999). Primary isolated HH40 stage chick aortic valve interstitial cells were treated with either scrambled control or siRNA against Cad-11 and embedded in a free floating 1% collagen gel as described previously (Richards et al., 2013). Cad-11 siRNA-treated cells compacted ~47% less (Fig. 3C, 24.5% vs. 16.7%, $p<0.05$). Together, these results suggest that Cad-11 deficiency affects valve mesenchymal/interstitial cell migration and traction force generation.

3.5. Cad-11 deficiency results in persistent immaturity of fetal aortic valve interstitial cells

We next profiled a panel of proteins involved with cell migration and contractile phenotype (Fig. 5). Vimentin is a marker of mature quiescent fibroblast phenotype, while alpha-smooth muscle actin (αSMA) is expressed in more immature mesenchymal cells (Butcher et al., 2007a). RhoA activity is involved in adhesion based signaling, and is critical for cell migration and traction force generation (Reffay et al., 2014). Traction forces are communicated to the extracellular matrix via integrins, of which the β1 component is commonly employed (Rahmouni et al., 2013). Immunohistochemical analysis determined that E18.5 wildtype aortic valves express vimentin, GTP-bound active RhoA (GTP-RhoA), and β1-integrin robustly, but with low levels of αSMA (Fig. 5A-D, I). Cad-11 $^{-/-}$ aortic valves however had 60–70% decreased vimentin, and further reduced active RhoA and β1 integrin expression by 3.0 and 2.5 fold, respectively. Interestingly, αSMA protein expression increased 2.4+/−0.2 fold, but was restricted to the endothelial edge of the valve leaflet (Fig. 5E–I). Together, these

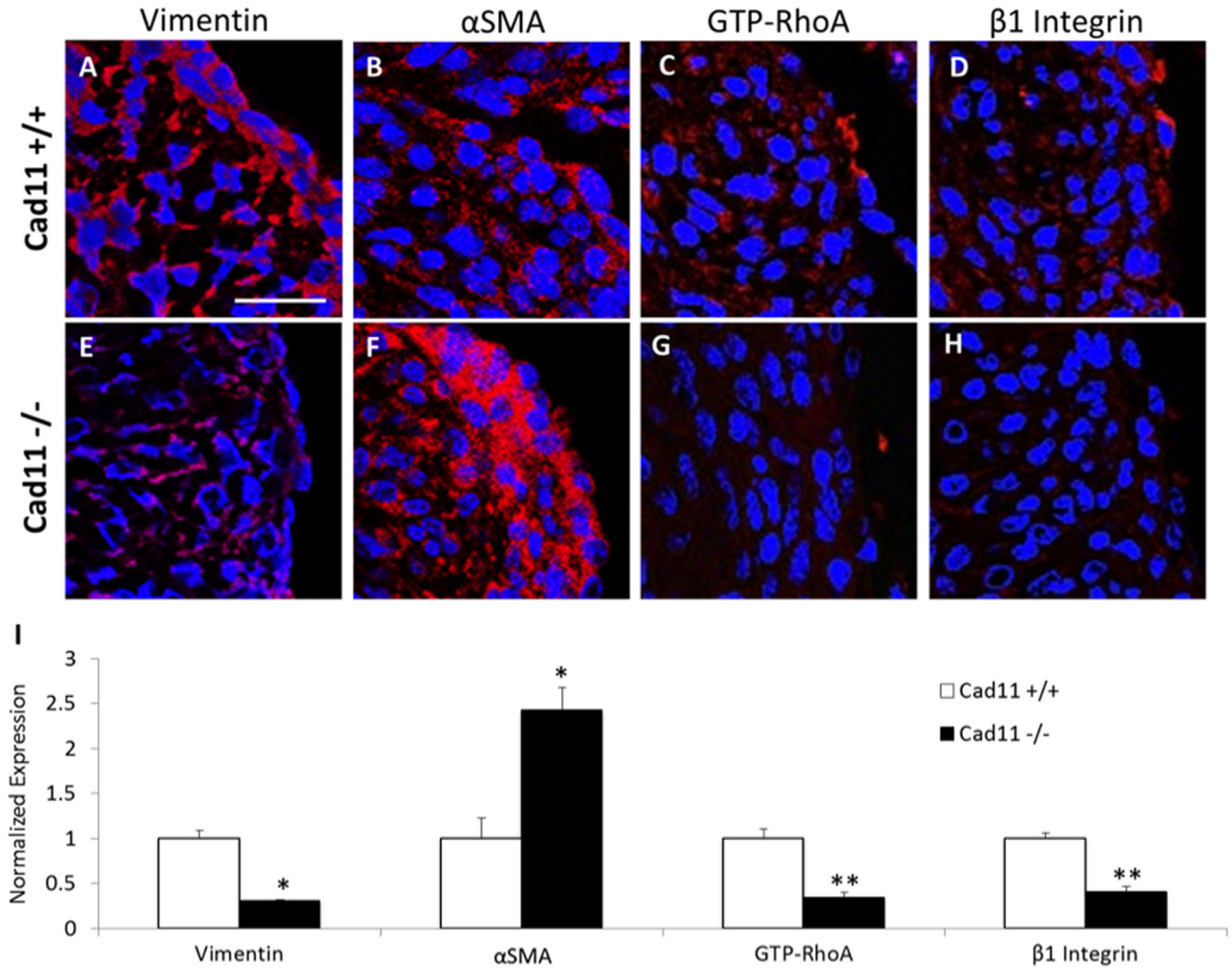

Fig. 5. Cad-11 deficiency results in persistent immaturity of fetal aortic valve interstitial cells. (A, C, D) Vimentin, GTP-RhoA, and β1 Integrin are all highly expressed in E18.5 Cad-11 $^{+/+}$ aortic valves. (E, G, H) There is little to no expression of these molecules in Cad-11 $^{-/-}$ valve cells. (B, F) αSMA expression is much higher in Cad-11 $^{-/-}$ cells as compared to control, but is concentrated at the endothelial edges of the valve leaflets. (I): Quantification of protein expression of wildtype and Cad-11 null aortic valves ($n \geq 3$, $^{*}p < 5E-3$, $^{**}p < 5E-4$) Scale bar = 25 μm.

suggest that Cad-11 deficiency results in a persistent immature valve mesenchymal phenotype in fetal aortic valves.

3.6. *Cad-11 controls cell polarity and collective migration in aortic valve interstitial cells through RhoA*

We further examined the migration ability of Cad-11 deficient cells in embedded spheroid culture (Duan et al., 2013). As previously mentioned, wildtype valve mesenchyme exhibited collective cell migration phenotype, with clusters of cells migrating together away from the central cell mass. In contrast, Cad-11 $^{-/-}$ cells exhibited no collective behavior (Fig. 4A vs. B, arrows), and were unable to migrate as far as controls (Fig. 4C). Cad-11 $^{-/-}$ cells extended single long processes radially outward from the cell mass in 3D culture, while wildtype cells displayed multiple filopodia (Fig. 4A and B). We next quantified filopodia extension and stress fiber formation characteristics of the primary VIC from murine Cad-11 wild type and null aortic valve interstitial cells in culture. While Cad-11 $^{+/+}$ cells exhibit many protrusions in many directions away from the cell body, Cad-11 $^{-/-}$ cells exhibit only 2–3 very long protrusions at the polar ends of the highly elongated cell (Fig. 4D–G). We then compared the activity of RhoA (GTP-bound) in both cell types. We found robust RhoA activity in the Cad- 11 $^{+/+}$ cells, with highest activity (determined by fluorescence intensity) within the filopodia. However, Cad-11 $^{-/-}$ cells expressed much less active RhoA, with barely any activity within filopodia (Fig. 4D and E). These findings suggested that RhoA activation during cell migration lies downstream of Cad-11. In 2D, Cad-11 deficient cells expressed significantly fewer stress fibers in comparison to controls, supporting that Cad-11 is important for directional migration and cell traction force generation (Fig. 6A and B). We thus hypothesized that restoring RhoA activity would rescue cellular activities caused by Cad-11 deficiency. Porcine aortic valve interstitial cells (PAVIC) were thus treated with either scrambled control, Cad-11 siRNA, or Cad-11 siRNA + CA-RhoA and subjected to the same morphology experiments. Similar to mouse valve interstitial cells and fetal chick valve mesenchyme, we observed fewer and longer protrusions in Cad-11 knockdown PAVIC compared to scrambled control cells (Fig. 6A–E). Cad-11 deficiency also increased the amount of cellular overlap, supporting that Cad-11 also controls contact inhibited locomotion (Fig. 6A–C and G). Induced expression of GTP-RhoA (via CA-RhoA transfection) increased cell protrusions, and decreased protrusion length (Fig. 6C and D). These cells also re-expressed stress fibers (arrows) and contact inhibited locomotion. Cad-11 siRNA treatment resulted in lower vimentin, RhoA, SOX9, and aggrecan gene expression, but

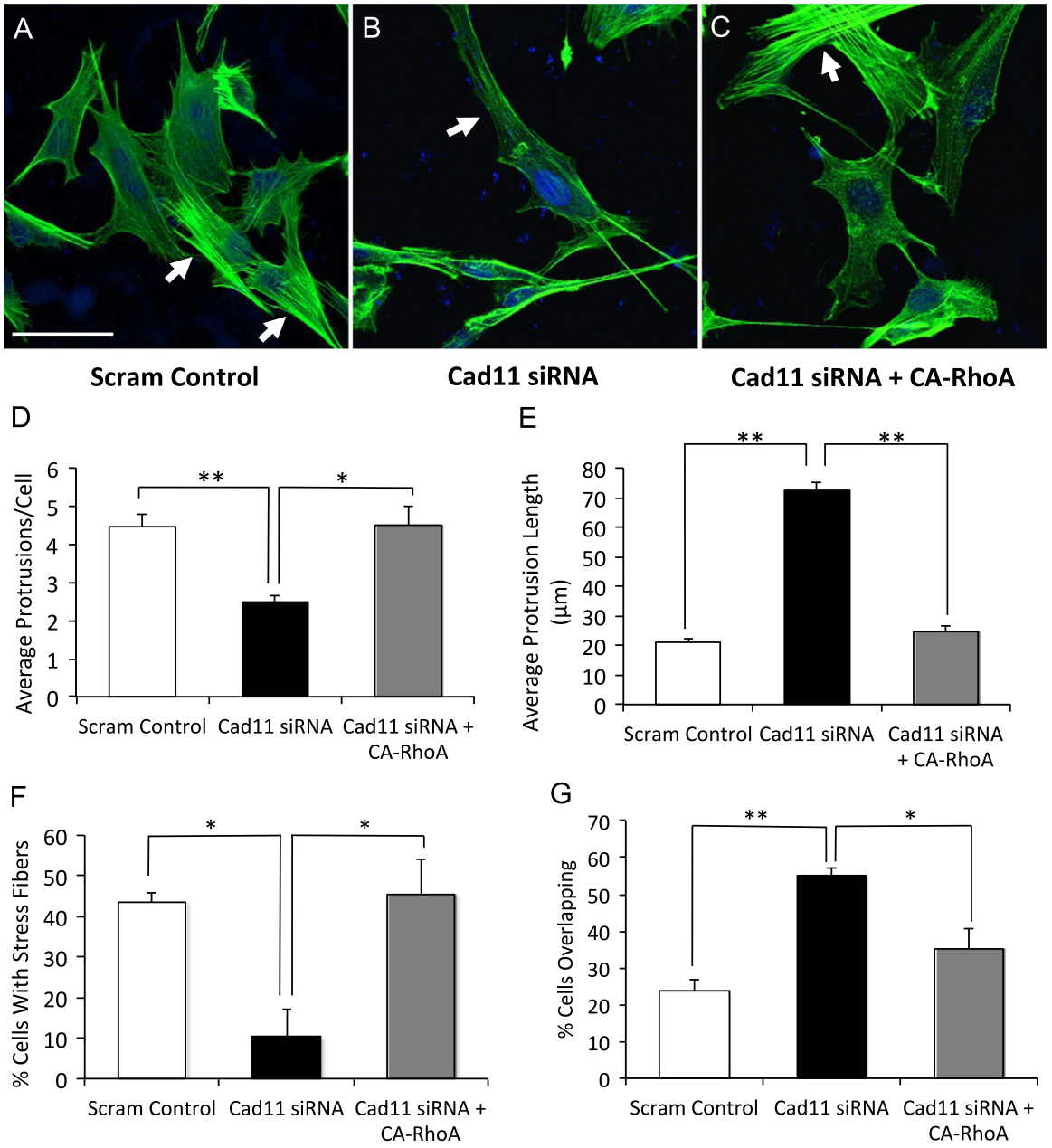

Fig. 6. Rescue of Cad-11 knockdown phenotype with CA-RhoA stained with F-actin. (A, B) Control PAVICs have about 4.5 protrusions per cell and a protrusion length of about 20 μm while Cad-11 knockdown PAVIC have fewer protrusions per cell, fewer stress fibers, and a much longer protrusion length. (C) Cad-11 knockdown + CA-RhoA PAVIC have similar phenotypes to the control PAVICs. ($n \geq 20$, $^{*}p < 0.005$, $^{**}p < 1E-20$). Scale bar = 50 μm (D–F) Re-expression of RhoA restores cell phenotypes and stress fiber formation ($n = 4$ groups of cells, $^{*}p < 0.05$), white arrows indicate stress fiber formation in control and siRNA/CA-RhoA treated cells and absence of stress fiber formation in siRNA-only treated cells. (G) Cad-11 null cells have a greater percentage of overlapping cells compared to control and rescue cells ($n = 4$ groups of cells, $^{*}p < 0.05$, $^{**}p < 0.0005$).

restoration of GTP-RhoA recovered vimentin, SOX9, and aggrecan at the mRNA level (Fig. S3). These results further support that RhoA activity is downstream of Cad-11 and is required for VIC filopodia extension, migration, and traction force generation.

3.7. *Adult Cad-11 $^{-/-}$ mice survivors have persistently thickened aortic valves and reduced RhoA activity, but do not calcify*

Given that homozygous deletion of Cad-11 produces some survivors, we examined the long-term consequences of Cad-11 deficiency on aortic valve structure and function in vivo. 10 month adult Cad-11 $^{-/-}$ aortic valves were 3.3 $^{+/-}$ 0.1 fold thicker than wildtype valves (Fig. 7A and B), establishing that morphological defects due to loss of Cad-11 persist postnatally into adulthood. Adult Cad-11 $^{-/-}$ aortic valves contained more cells than wildtype valves, but had no differences in cell density (Fig. 7D and H). We did not find differences in proliferation or apoptosis (as a percentage of total cells), supporting that any hypercellularization is not due to an increased cell density, but rather compensatory cell proliferation to accommodate the increased valve size (Fig. S1). Thickened valve leaflets are typically associated with calcific aortic valve disease, and we previously showed that Cad-11 expression is highly correlated with calcific valve disease in mice and humans (Zhou et al., 2013). We therefore analyzed calcification in Cad-11 $^{+/+}$ vs. Cad-11 $^{-/-}$ aortic valves. We found a few small Von Kossa positive phosphate lesions in 10-month WT mice (Fig. 7E, arrows), which was anticipated from previous reports (Tanaka et al., 2005). However, we found no detectable staining in Cad-11 $^{-/-}$ valves

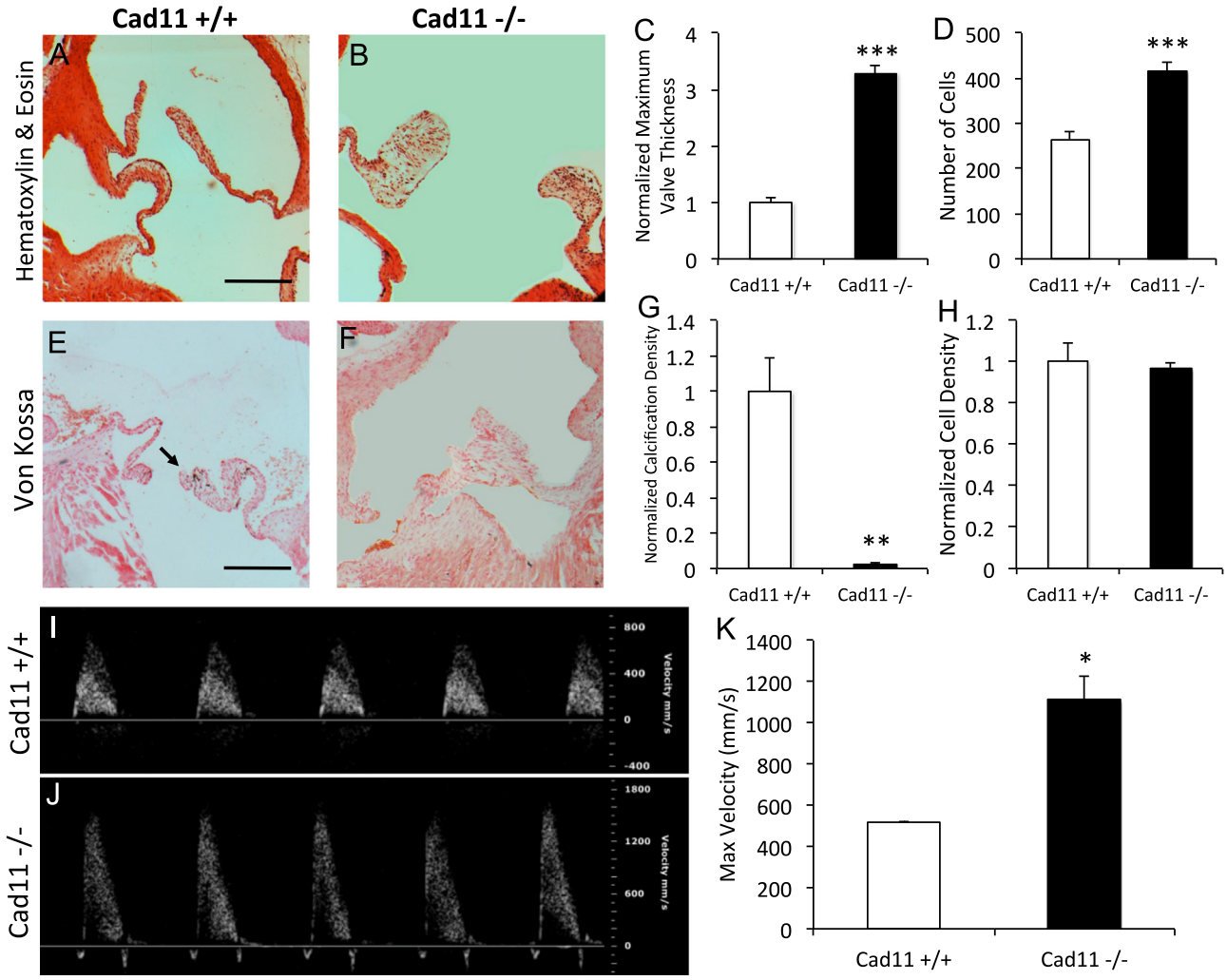

Fig. 7. Defects due to loss of cadherin-11 persist throughout adulthood. (A–D, H) Cad-11 $^{-/-}$ aortic valve leaflets (B) are significantly thicker than Cad-11 $^{+/+}$ leaflets (A) ($n=5$, $^{***}p<1E-4$). Cad-11 $^{-/-}$ valves have similar cell density to Cad-11 $^{+/+}$, but contain more cells ($n=4$, $^{***}p<1E-4$). (E–G) Calcification of 10 month old adult valve leaflets does not occur with loss of cadherin-11 (F) but does occur minimally in Cad-11 $^{+/+}$ leaflets (E) ($n=3$, $^{**}p<0.001$) Scale bar=0.2 mm (I–K) Cad-11 $^{-/-}$ mice have increased maximum ejection velocity through the aortic valve compared to Cad-11 $^{+/+}$ mice at 10 months ($n=3$, $^{*}p<0.05$).

despite significant thickening (Fig. 7E vs. F). This finding is consistent with our previous studies associating elevated Cad-11 with aortic valve calcification. Interestingly, Pulse wave Doppler ultrasound revealed that Cad-11 $^{-/-}$ adults had elevated ejection velocity through the aortic valve, indicating hemodynamically relevant aortic valve stenosis as a result of thickened valves without evidence of pathological extracellular matrix remodeling (Fig. 7I–K). These results suggest that a loss of Cad-11 in adulthood could be protective against pathological remodeling and stenosis, however residual effects of earlier valve deformations still cause hemodynamically relevant disease. Cad-11 $^{-/-}$ leaflets expressed more extracellular matrix than wildtype controls, but histological analysis revealed no differences in relative amounts of glycosaminoglycans, collagen, or elastin (Figs. 8A, B and S2). In contrast to fetal valves, nuclear expression of SOX9 was similar in both Cad-11 $^{+/+}$ and Cad-11 $^{-/-}$ aortic valves in 10-month-old adult mice (Fig. 8A–D). RhoA activity in 10-month old valves was elevated in comparison to the fetal stage, but GTP-RhoA remained significantly decreased in the Cad-11 $^{-/-}$ valve leaflets (Fig. 8E and F). These findings support that adult Cad-11 deficient aortic valves remain pathologically thickened and functionally stenotic, but resistant to calcification.

4. Discussion

Long-term efficient cardiac performance requires that the heart valves consistently restrict retrograde blood flow while posing near negligible resistance to forward flow. This diode-like function becomes progressively disrupted during disease pathogenesis, leading to stenosis and regurgitation. It is increasingly more appreciated that the same molecular mechanisms that participate in the formation of heart valves are also reactivated during disease, in particular calcification of the aortic valve (Wirrig and Yutzey, 2011). However, the mechanisms by which cells interact with their tissue environment during these remodeling processes are less understood. We previously identified the cell–cell adhesion protein cadherin-11 as uniquely expressed in aortic valve endothelium (Butcher et al., 2006). More recently, we and others determined that differential expression of Cad-11 at various stages of valvulogenesis and during postnatal disease suggests that Cad-11 is important for aortic valve tissue formation and remodeling (Hutcheson et al., 2013; Zhou et al., 2013). In this study, we identified how Cad-11 coordinates cellular activities during embryonic valve formation and in postnatal valve homeostasis. We determined that in Cad-11 $^{-/-}$ embryos, initial EMT does occur, however the migrating cells remain close to the endocardium and do not populate the cushions evenly. Post-EMT valve remodeling is

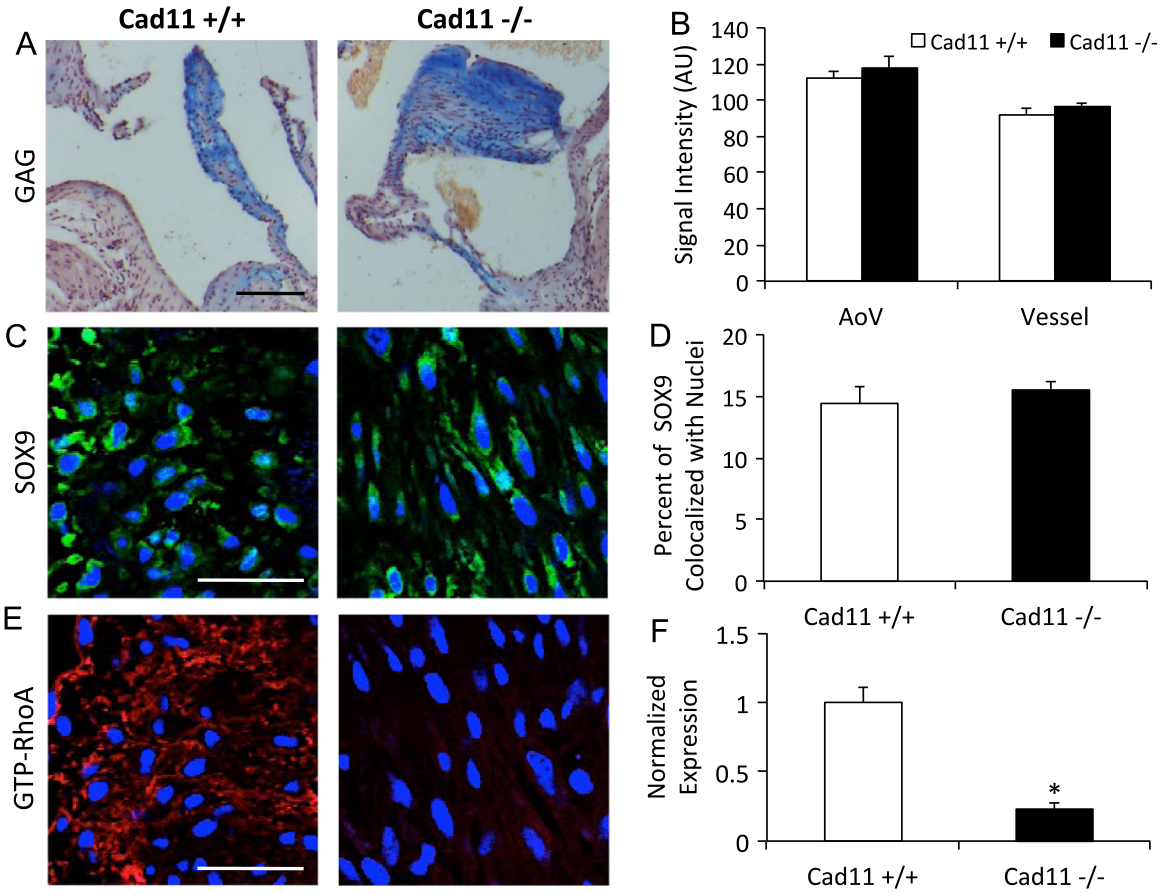

Fig. 8. Cad-11 null mice and wildtype mice have no differences in GAGs in aortic valve leaflets at 10 months. (A, B) Alcian blue staining shows no differences in GAG intensity in Cad-11 null mouse aortic valves compared to control valves ($n=4$, $p=0.46$). Scale bar = 100 μm (C, D) SOX9 is equally colocalized with nuclei in both wildtype and Cad-11 null mice, suggesting there exists a compensatory mechanism involving SOX9 that restores GAG production. There were no differences in whole valve SOX9 expression (graph not shown), ($n=4$, $p=0.50$). Scale bar = 25 μm (E, F) Postnatal active RhoA deficiency for Cad-11 null mice persists into adulthood. ($n=4$, $^{*}p < 1E-5$) Scale bar = 25 μm.

also significantly affected, and loss of Cad-11 may affect other cell types in the heart as well, which also contribute to post-EMT valve remodeling. Additionally, early embryonic cushions have regions of hypercellularity (immediately subendothelial) and regions of hypocellularity (near the myocardial border), and this heterogeneous cell density likely contributed to downstream malformation and poor remodeling. Most mice die between E14.5 and birth with severely thickened semilunar valve leaflets, however those that survive are able to compensate to develop sufficiently functional valves but with a consequence of chronic deficiency in remodeling. Cad-11 depleted valve cells were unable to migrate collectively, exhibited markedly impaired filopodia extension, and limited stress fiber formation. Cad-11 loss was associated with reduced RhoA activity regardless of age of the tissue. RhoA activity restoration however was sufficient to rescue stress fiber formation, filipodia extension, and phenotypic gene expression. These findings elevate the role of mesenchymal cell–cell adhesive signaling for proper heart valve formation and homeostatic remodeling.

After endocardial to mesenchymal transformation, embryonic valvular progenitors migrate away from the endocardial surface and invade the cardiac jelly space to create the endocardial cushions (Kinsella and Fitzharris, 1980). This process occurs over an approximately 72-h period in the chick and the mouse. Primary migrating mesenchyme secrete proteoglycans that promote endocardial detachment and enable paths for trailing cells to follow (Markwald et al., 1981). Though spatial and temporal asymmetries exist in the distribution of mesenchyme within the cushions, cellularization largely resembles a front of collectively migrating cells that progresses towards the myocardial border (Bernanke and Markwald, 1979, 1984; Moreno-Rodriguez et al., 1997). Directional collective cell migration is essential for multiple morphogenic events, including neural crest migration and specification to craniofacial tissues (Borchers et al., 2001). Most EMT derived mesenchymal cells maintain epithelial cell–cell adhesion molecules transiently at their surface, suggesting that they maintain some ability to interact with their neighbors, which may initiate collective migratory behavior (Theveneau and Mayor, 2013). Mesenchymal cells also express cadherins, including N-cadherin and Cadherin-11, that form cadherin-based adherens junctions (Theveneau et al., 2010). Our findings of restricted migration of mesenchymal progenitors from the endocardial boundary in vivo combined with the lack of contact inhibited locomotion and collective migration in vitro supports that these mesenchymal progenitors require Cad-11 to regulate intercellular communication and migration guidance during this process.

Cadherin signaling regulates cell protrusion formation and functions upstream of small GTPases CDC42, RAC1, and RhoA (Barth et al., 2009; Borghi et al., 2010; Maruthamuthu et al., 2010). GTPase activity is highly specific and spatially localized within the cell. For example, Rac1 controls leading edge filopodia extension and polarity generation, while RhoA controls rear-edge filopodia retraction and cell contraction (Theveneau and Mayor, 2013). Cadherin-binding mediated signaling through a variety of adherens junction accessory proteins coordinate RhoA and Rac1 expression proteins to promote efficient collision driven collective migration requiring both co-attraction and contact inhibited locomotion (Kashef et al., 2009; Niessen et al., 2011). Restoration of the constitutively active (CA), but not dominant-negative, form of

the small GTPases via embryo injection rescued protrusion formation (Kashef et al., 2009). In our application, expression of CA-RhoA was sufficient to restore stress fiber formation, filopodia extension, and ECM gene expression, supporting that RhoA acts downstream of Cad-11 to coordinate sensation into migratory responses. This is not to say that other GTPase activities could be involved. For example, RAC1 has also been shown to rescue decreases in migration ability due to loss of Cad-11 in neural crest cells (Theveneau et al., 2010). Cad-11 binding mediates these activities through its interaction with RhoA/Rac1 at P120 or through competition with Wnt/PCP signaling by sequestering β-catenin (Boguslavsky et al., 2007; Rimm et al., 1995). Indeed, cell polarity is disrupted by either Cad-11 deficiency or overexpression of Wnt signaling via constitutively activating disheveled, and is rescued by forced activation of RhoA or Rac1 (Koehler et al., 2013). GTPase activity is further modified by integrin mediated focal adhesion complex proteins to migrate and remodel matrix, including filaminA, FilGAP, and CdGAP (Duval et al., 2014; LaLonde et al., 2006; Ohta et al., 2006). Importantly, small GTPase signaling interacts with known valvulogenic signaling pathways, including TGFβ and Wnt/β-catenin (Chen et al., 2011; Mercado-Pimentel et al., 2007). More likely a complex dynamic of cell–cell and cell-matrix adhesion coordinates formation and stabilization of the endocardial cushion, and assessing the specific roles of each is an important remaining question.

Cellular compaction of the endocardial cushions is critical for fetal valve remodeling to create thin, fibrous leaflets that prevent regurgitation under increasing hemodynamic loads (Phoon et al., 2004). Ultrasound determined that the aortic valves of Cad-11 $^{-/-}$ fetal mice were mechanically insufficient, and histology confirmed the tissue was markedly thickened. We verified the inability of aortic valve mesenchyme to compact 3D matrix after Cad-11 knockdown, which supports that the functional capacity of valves to remodel is severely diminished post-EMT. The mechanism for this deficiency is not yet fully elucidated, but evidence suggests a role for impaired mechanosensation, potentially via RhoA. We previously showed Rho kinase inhibition disrupts 3D matrix compaction of atrioventricular mesenchymal cells (Butcher et al., 2007a). Activation of RhoA by LPA induced cushion stiffening and ECM deposition, while rho kinase blockade inhibited both (Tan et al., 2013). Cad-11 signaling may also affect interact with other signaling programs, one example of which could be TGFβ. We recently showed that exogenous TGFβ3 induces atrioventricular cushion stiffening while limiting its compaction (Buskohl et al., 2012). Similarly, Hutcheson et al. (2013) determined TGFβ1 stimulation increased cellular tension and Cad-11 expression in adult aortic valve interstitial cells. Cad-11 withstands 2x the dissociation force of N-cadherin (another important mesenchymal cadherin), and requires much lower calcium concentrations to act (Pittet et al., 2008). Conversely, Cad-11 expression decreases in the interstitium during normal fetal valve remodeling but is maintained in the endothelium, which indicates that Cad-11 may exhibit different functions within each cell type during valvular morphogenesis (Zhou et al., 2013).

The function of Cad-11 in postnatal valve homeostasis remains largely unknown. Cad-11 expression is restricted to the endothelium in healthy valves, but is reactivated in the interstitium during calcific degeneration. TGFβ mediated Cad-11 expression coordinates valve interstitial cell aggregation and nodule formation in vitro through increased cell–cell tension (Hutcheson et al., 2013), but whether this progresses to calcification remains unclear (Cloyd et al., 2012). We found in this study that the few postnatal Cad-11 $^{-/-}$ survivors maintained persistently thickened aortic valves, but relatively normal proportions of ECM expression. These valves had decreased RhoA activity, but normal Sox9 expression compared to wildtype controls. Interestingly, the adult valves were no longer regurgitant, but hemodynamically stenotic. Furthermore, we found a few small calcific lesions in 10 month wildtype valves, but none were found in Cad-11 $^{-/-}$ aortic valves. These findings suggest that the lack of Cad-11 still compromises the ability of postnatal valves to properly sense their mechanical environment and remodel the tissue accordingly, but manages to avoid calcific degeneration. Cad-11 therefore exerts multiple influences on resident cell behavior, including cell contractile phenotype, sensation of external microenvironment, and production/maturation of extracellular matrix. The mechanism for this is not yet elucidated, but may be related to impaired cellular mechanosensation. We previously identified Cad-11 as uniquely expressed in valve endothelium and was shear stress sensitive (Butcher et al., 2006), but valves also experience cyclic stretch and pressure loads. Given the strong relationship between valve morphology and function, our results suggest that well controlled mechanical signaling and feedback response is essential for maintenance of aortic valve tissue homeostasis. Indeed, mechanical conditioning of de novo engineered valve tissues induces mechanical strengthening and biological maturation, both of which are predictive of in vivo performance (Rabkin-Aikawa et al., 2004).

5. Conclusions

In this study, we establish essential roles for Cad-11 for collective migration of mesenchymal progenitors in forming the endocardial cushion and its subsequent compaction into thin fibrous leaflets. We also identified RhoA activity downstream of Cad-11 as sufficient to control the migratory and traction force generation for these morphogenic behaviors. Finally, we determined that lack of Cad-11 results in persistently malformed valves, but protection from calcification. These results support that Cad-11 is an important mechanosensory component regulating heart valve morphogenesis and tissue homeostasis, misexpression of which leads to congenital and postnatal valve dysfunction.

Acknowledgments

This study was supported by the National Institutes of Health (HL110328 and HL18672 to JTB) and National Science Foundation (CBET-0955712 to JTB), the American Heart Association Undergraduate Student Fellowship (CJB) and Hunter R. Rawlings III Cornell Presidential Research Scholarship (CJB and DCS). We thank Andrew Recknagel for his technical expertize.

Appendix A. Supplementary information

Supplementary data associated with this article can be found in the online version at http://dx.doi.org/10.1016/j.ydbio.2015.07.012.

References

Aikawa, E., Whittaker, P., Farber, M., Mendelson, K., Padera, R.F., Aikawa, M., Schoen, F.J., 2006. Human semilunar cardiac valve remodeling by activated cells from fetus to adult: implications for postnatal adaptation, pathology, and tissue engineering. Circulation 113, 1344–1352.

Assefnia, S., Dakshanamurthy, S., Guidry Auvil, J.M., Hampel, C., Anastasiadis, P.Z., Kallakury, B., Uren, A., Foley, D.W., Brown, M.L., Shapiro, L., Brenner, M., Haigh, D., Byers, S.W., 2014. Cadherin-11 in poor prognosis malignancies and rheumatoid arthritis: common target, common therapies. Oncotarget 5, 1458–1474.

Azhar, M., Brown, K., Gard, C., Chen, H., Rajan, S., Elliott, D.A., Stevens, M.V., Camenisch, T.D., Conway, S.J., Doetschman, T., 2011. Transforming growth factor Beta2 is required for valve remodeling during heart development. Dev. Dyn. 240, 2127–2141.

Barth, M., Schumacher, H., Kuhn, C., Akhyari, P., Lichtenberg, A., Franke, W.W., 2009. Cordial connections: molecular ensembles and structures of adhering junctions connecting interstitial cells of cardiac valves in situ and in cell culture. Cell Tissue Res. 337, 63–77.
Bartman, T., Hove, J., 2005. Mechanics and function in heart morphogenesis. Dev. Dyn. 233, 373–381.
Becker, S.F., Mayor, R., Kashef, J., 2013. Cadherin-11 mediates contact inhibition of locomotion during Xenopus neural crest cell migration. PLoS One 8, e85717.
Bernanke, D.H., Markwald, R.R., 1979. Effects of hyaluronic acid on cardiac cushion tissue cells in collagen matrix cultures. Tex. Rep. Biol. Med. 39, 271–285.
Bernanke, D.H., Markwald, R.R., 1984. Effects of two glycosaminoglycans on seeding of cardiac cushion tissue cells into a collagen-lattice culture system. Anat. Rec. 210, 25–31.
Boguslavsky, S., Grosheva, I., Landau, E., Shtutman, M., Cohen, M., Arnold, K., Feinstein, E., Geiger, B., Bershadsky, A., 2007. p120 catenin regulates lamellipodial dynamics and cell adhesion in cooperation with cortactin. Proc. Natl. Acad. Sci. USA 104, 10882–10887.
Borchers, A., David, R., Wedlich, D., 2001. Xenopus cadherin-11 restrains cranial neural crest migration and influences neural crest specification. Development 128, 3049–3060.
Borghi, N., Lowndes, M., Maruthamuthu, V., Gardel, M.L., Nelson, W.J., 2010. Regulation of cell motile behavior by crosstalk between cadherin- and integrin-mediated adhesions. Proc. Natl. Acad. Sci. USA 107, 13324–13329.
Buskohl, P.R., Sun, M.L., Thompson, R.P., Butcher, J.T., 2012. Serotonin potentiates transforming growth factor-beta3 induced biomechanical remodeling in avian embryonic atrioventricular valves. PLoS One 7, e42527.
Butcher, J.T., Nerem, R.M., 2004. Porcine aortic valve interstitial cells in three-dimensional culture: comparison of phenotype with aortic smooth muscle cells. J. Heart Valve Dis. 13, 478–485, discussion 485-476..
Butcher, J.T., Norris, R.A., Hoffman, S., Mjaatvedt, C.H., Markwald, R.R., 2007a. Periostin promotes atrioventricular mesenchyme matrix invasion and remodeling mediated by integrin signaling through Rho/PI 3-kinase. Dev. Biol. 302, 256–266.
Butcher, J.T., Sedmera, D., Guldberg, R.E., Markwald, R.R., 2007b. Quantitative volumetric analysis of cardiac morphogenesis assessed through micro-computed tomography. Dev. Dyn. 236, 802–809.
Butcher, J.T., Tressel, S., Johnson, T., Turner, D., Sorescu, G., Jo, H., Nerem, R.M., 2006. Transcriptional profiles of valvular and vascular endothelial cells reveal phenotypic differences: influence of shear stress. Arterioscler. Thromb. Vasc. Biol. 26, 69–77.
Chakraborty, S., Combs, M.D., Yutzey, K.E., 2010. Transcriptional regulation of heart valve progenitor cells. Pediatr. Cardiol. 31, 414–421.
Chen, J.H., Chen, W.L., Sider, K.L., Yip, C.Y., Simmons, C.A., 2011. Beta-catenin mediates mechanically regulated, transforming growth factor-beta1-induced myofibroblast differentiation of aortic valve interstitial cells. Arterioscler. Thromb. Vasc. Biol. 31, 590–597.
Cloyd, K.L., El-Hamamsy, I., Boonrungsiman, S., Hedegaard, M., Gentleman, E., Sarathchandra, P., Colazzo, F., Gentleman, M.M., Yacoub, M.H., Chester, A.H., Stevens, M.M., 2012. Characterization of porcine aortic valvular interstitial cell 'calcified' nodules. PLoS One 7, e48154.
Duan, B., Hockaday, L.A., Kapetanovic, E., Kang, K.H., Butcher, J.T., 2013. Stiffness and adhesivity control aortic valve interstitial cell behavior within hyaluronic acid based hydrogels. Acta Biomater. 9, 7640–7650.
Duval, D., Lardeux, A., Le Tourneau, T., Norris, R.A., Markwald, R.R., Sauzeau, V., Probst, V., Le Marec, H., Levine, R., Schott, J.J., Merot, J., 2014. Valvular dystrophy associated filamin A mutations reveal a new role of its first repeats in small-GTPase regulation. Biochim. Biophys. Acta 1843, 234–244.
Eisenberg, L.M., Markwald, R.R., 1995. Molecular regulation of atrioventricular valvuloseptal morphogenesis. Circ. Res. 77, 1–6.
Farrar, E.J., Butcher, J.T., 2013. Heterogeneous susceptibility of valve endothelial cells to mesenchymal transformation in response to TNFalpha. Ann. Biomed. Eng. 42, 149–161.
Galvin, K.M., Donovan, M.J., Lynch, C.A., Meyer, R.I., Paul, R.J., Lorenz, J.N., Fairchild-Huntress, V., Dixon, K.L., Dunmore, J.H., Gimbrone Jr., M.A., Falb, D., Huszar, D., 2000. A role for smad6 in development and homeostasis of the cardiovascular system. Nat. Genet. 24, 171–174.
Ghatak, S., Misra, S., Norris, R.A., Moreno-Rodriguez, R.A., Hoffman, S., Levine, R.A., Hascall, V.C., Markwald, R.R., 2014. Periostin induces intracellular cross-talk between kinases and hyaluronan in atrioventricular valvulogenesis. J. Biol. Chem. 289, 8545–8561.
Gould, R.A., Chin, K., Santisakultarm, T.P., Dropkin, A., Richards, J.M., Schaffer, C.B., Butcher, J.T., 2012. Cyclic strain anisotropy regulates valvular interstitial cell phenotype and tissue remodeling in three-dimensional culture. Acta Biomater. 8, 1710–1719.
Grinnell, F., Ho, C.H., Lin, Y.C., Skuta, G., 1999. Differences in the regulation of fibroblast contraction of floating versus stressed collagen matrices. J. Biol. Chem. 274, 918–923.
Hinton Jr., R.B., Lincoln, J., Deutsch, G.H., Osinska, H., Manning, P.B., Benson, D.W., Yutzey, K.E., 2006. Extracellular matrix remodeling and organization in developing and diseased aortic valves. Circ. Res. 98, 1431–1438.
Hoffman, J.I., Kaplan, S., Liberthson, R.R., 2004. Prevalence of congenital heart disease. Am. Heart J. 147, 425–439.
Hoffmann, I., Balling, R., 1995. Cloning and expression analysis of a novel mesodermally expressed cadherin. Dev. Biol. 169, 337–346.
Hu, N., Clark, E.B., 1989. Hemodynamics of the stage 12 to stage 29 chick embryo. Circ. Res. 65, 1665–1670.
Hutcheson, J.D., Chen, J., Sewell-Loftin, M.K., Ryzhova, L.M., Fisher, C.I., Su, Y.R., Merryman, W.D., 2013. Cadherin-11 regulates cell–cell tension necessary for calcific nodule formation by valvular myofibroblasts. Arterioscler. Thromb. Vasc. Biol. 33, 114–120.
Kashef, J., Kohler, A., Kuriyama, S., Alfandari, D., Mayor, R., Wedlich, D., 2009. Cadherin-11 regulates protrusive activity in Xenopus cranial neural crest cells upstream of Trio and the small GTPases. Genes Dev. 23, 1393–1398.
Kawaguchi, J., Azuma, Y., Hoshi, K., Kii, I., Takeshita, S., Ohta, T., Ozawa, H., Takeichi, M., Chisaka, O., Kudo, A., 2001. Targeted disruption of cadherin-11 leads to a reduction in bone density in calvaria and long bone metaphyses. J. Bone Miner. Res. 16, 1265–1271.
Keller, B.B., Hu, N., Serrino, P.J., Clark, E.B., 1991. Ventricular pressure-area loop characteristics in the stage 16 to 24 chick embryo. Circ. Res. 68, 226–231.
Kinsella, M.G., Fitzharris, T.P., 1980. Origin of cushion tissue in the developing chick heart: cinematographic recordings of in situ formation. Science 207, 1359–1360.
Koehler, A., Schlupf, J., Schneider, M., Kraft, B., Winter, C., Kashef, J., 2013. Loss of Xenopus cadherin-11 leads to increased Wnt/beta-catenin signaling and up-regulation of target genes c-myc and cyclin D1 in neural crest. Dev. Biol. 383, 132–145.
Kruithof, B.P., Krawitz, S.A., Gaussin, V., 2007. Atrioventricular valve development during late embryonic and postnatal stages involves condensation and extracellular matrix remodeling. Dev. Biol. 302, 208–217.
LaLonde, D.P., Grubinger, M., Lamarche-Vane, N., Turner, C.E., 2006. CdGAP associates with actopaxin to regulate integrin-dependent changes in cell morphology and motility. Curr. Biol. 16, 1375–1385.
Lee, D.M., Kiener, H.P., Agarwal, S.K., Noss, E.H., Watts, G.F., Chisaka, O., Takeichi, M., Brenner, M.B., 2007. Cadherin-11 in synovial lining formation and pathology in arthritis. Science 315, 1006–1010.
Lee, Y.M., Cope, J.J., Ackermann, G.E., Goishi, K., Armstrong, E.J., Paw, B.H., Bischoff, J., 2006. Vascular endothelial growth factor receptor signaling is required for cardiac valve formation in zebrafish. Dev. Dyn. 235, 29–37.
Lin, C.Y., Lin, C.J., Chen, C.H., Chen, R.M., Zhou, B., Chang, C.P., 2012. The secondary heart field is a new site of calcineurin/Nfatc1 signaling for semilunar valve development. J. Mol. Cell. Cardiol. 52, 1096–1102.
Lincoln, J., Kist, R., Scherer, G., Yutzey, K.E., 2007. Sox9 is required for precursor cell expansion and extracellular matrix organization during mouse heart valve development. Dev. Biol. 305, 120–132.
Mahler, G.J., Farrar, E.J., Butcher, J.T., 2013. Inflammatory cytokines promote mesenchymal transformation in embryonic and adult valve endothelial cells. Arterioscler. Thromb. Vasc. Biol. 33, 121–130.
Markwald, R.R., Krook, J.M., Kitten, G.T., Runyan, R.B., 1981. Endocardial cushion tissue development: structural analyses on the attachment of extracellular matrix to migrating mesenchymal cell surfaces. Scan Electron Microsc. 2, 261–274.
Maruthamuthu, V., Aratyn-Schaus, Y., Gardel, M.L., 2010. Conserved F-actin dynamics and force transmission at cell adhesions. Curr. Opin. Cell Biol. 22, 583–588.
Mercado-Pimentel, M.E., Hubbard, A.D., Runyan, R.B., 2007. Endoglin and Alk5 regulate epithelial-mesenchymal transformation during cardiac valve formation. Dev. Biol. 304, 420–432.
Mo, F.E., Lau, L.F., 2006. The matricellular protein CCN1 is essential for cardiac development. Circ. Res. 99, 961–969.
Moreno-Rodriguez, R.A., de la Cruz, M.V., Krug, E.L., 1997. Temporal and spatial asymmetries in the initial distribution of mesenchyme cells in the atrioventricular canal cushions of the developing chick heart. Anat. Rec. 248, 84–92.
Niessen, C.M., Leckband, D., Yap, A.S., 2011. Tissue organization by cadherin adhesion molecules: dynamic molecular and cellular mechanisms of morphogenetic regulation. Physiol. Rev. 91, 691–731.
Ohta, Y., Hartwig, J.H., Stossel, T.P., 2006. FilGAP, a Rho- and ROCK-regulated GAP for Rac binds filamin A to control actin remodelling. Nat. Cell Biol. 8, 803–814.
Person, A.D., Klewer, S.E., Runyan, R.B., 2005. Cell biology of cardiac cushion development. Int. Rev. Cytol. 243, 287–335.
Phoon, C.K., Ji, R.P., Aristizabal, O., Worrad, D.M., Zhou, B., Baldwin, H.S., Turnbull, D. H., 2004. Embryonic heart failure in NFATc1 −/− mice: novel mechanistic insights from in utero ultrasound biomicroscopy. Circ. Res. 95, 92–99.
Pittet, P., Lee, K., Kulik, A.J., Meister, J.J., Hinz, B., 2008. Fibrogenic fibroblasts increase intercellular adhesion strength by reinforcing individual OB-cadherin bonds. J. Cell Sci. 121, 877–886.
Rabkin-Aikawa, E., Farber, M., Aikawa, M., Schoen, F.J., 2004. Dynamic and reversible changes of interstitial cell phenotype during remodeling of cardiac valves. J. Heart Valve Dis. 13, 841–847.
Rahmouni, S., Lindner, A., Rechenmacher, F., Neubauer, S., Sobahi, T.R., Kessler, H., Cavalcanti-Adam, E.A., Spatz, J.P., 2013. Hydrogel micropillars with integrin selective peptidomimetic functionalized nanopatterned tops: a new tool for the measurement of cell traction forces transmitted through alphavbeta3- or alpha5beta1-integrins. Adv. Mater. 25, 5869–5874.
Reffay, M., Parrini, M.C., Cochet-Escartin, O., Ladoux, B., Buguin, A., Coscoy, S., Amblard, F., Camonis, J., Silberzan, P., 2014. Interplay of RhoA and mechanical forces in collective cell migration driven by leader cells. Nat. Cell Biol. 16, 217–223.
Richards, J., El-Hamamsy, I., Chen, S., Sarang, Z., Sarathchandra, P., Yacoub, M.H., Chester, A.H., Butcher, J.T., 2013. Side-specific endothelial-dependent regulation of aortic valve calcification: interplay of hemodynamics and nitric oxide signaling. Am. J. Pathol. 182, 1922–1931.
Rimm, D.L., Koslov, E.R., Kebriaei, P., Cianci, C.D., Morrow, J.S., 1995. Alpha 1(E)-

catenin is an actin-binding and -bundling protein mediating the attachment of F-actin to the membrane adhesion complex. Proc. Natl. Acad. Sci. USA 92, 8813–8817.
Sacks, M.S., Schoen, F.J., 2002. Collagen fiber disruption occurs independent of calcification in clinically explanted bioprosthetic heart valves. J. Biomed. Mater. Res. 62, 359–371.
Sakata, Y., Kamei, C.N., Nakagami, H., Bronson, R., Liao, J.K., Chin, M.T., 2002. Ventricular septal defect and cardiomyopathy in mice lacking the transcription factor CHF1/Hey2. Proc. Natl. Acad. Sci .USA 99, 16197–16202.
Schneider, D.J., Wu, M., Le, T.T., Cho, S.H., Brenner, M.B., Blackburn, M.R., Agarwal, S. K., 2012. Cadherin-11 contributes to pulmonary fibrosis: potential role in TGF-beta production and epithelial to mesenchymal transition. FASEB J. 26, 503–512.
Simonneau, L., Kitagawa, M., Suzuki, S., Thiery, J.P., 1995. Cadherin 11 expression marks the mesenchymal phenotype: towards new functions for cadherins? Cell Adhes. Commun. 3, 115–130.
Tan, H., Biechler, S., Junor, L., Yost, M.J., Dean, D., Li, J., Potts, J.D., Goodwin, R.L., 2013. Fluid flow forces and rhoA regulate fibrous development of the atrioventricular valves. Dev. Biol. 374, 345–356.
Tanaka, K., Sata, M., Fukuda, D., Suematsu, Y., Motomura, N., Takamoto, S., Hirata, Y., Nagai, R., 2005. Age-associated aortic stenosis in apolipoprotein E-deficient mice. J. Am. Coll. Cardiol. 46, 134–141.
Tatin, F., Taddei, A., Weston, A., Fuchs, E., Devenport, D., Tissir, F., Makinen, T., 2013. Planar cell polarity protein Celsr1 regulates endothelial adherens junctions and directed cell rearrangements during valve morphogenesis. Dev. Cell 26, 31–44.
Theveneau, E., Marchant, L., Kuriyama, S., Gull, M., Moepps, B., Parsons, M., Mayor, R., 2010. Collective chemotaxis requires contact-dependent cell polarity. Dev. Cell 19, 39–53.
Theveneau, E., Mayor, R., 2013. Collective cell migration of epithelial and mesenchymal cells. Cell. Mol. Life Sci. 70, 3481–3492.
Tomita, K., van Bokhoven, A., van Leenders, G.J., Ruijter, E.T., Jansen, C.F., Bussemakers, M.J., Schalken, J.A., 2000. Cadherin switching in human prostate cancer progression. Cancer Res. 60, 3650–3654.
Townsend, T.A., Robinson, J.Y., Deig, C.R., Hill, C.R., Misfeldt, A., Blobe, G.C., Barnett, J. V., 2011. BMP-2 and TGFbeta2 shared pathways regulate endocardial cell transformation. Cells Tissues Organs 194, 1–12.
Wirrig, E.E., Yutzey, K.E., 2011. Transcriptional regulation of heart valve development and disease. Cardiovasc. Pathol. 20, 162–167.
Zhou, J., Bowen, C., Lu, G., Knapp Iii, C., Recknagel, A., Norris, R.A., Butcher, J.T., 2013. Cadherin-11 expression patterns in heart valves associate with key functions during embryonic cushion formation, valve maturation and calcification. Cells Tissues Organs 198, 300–310.